Chemical Engineering Journal 101 (2004) 315–322

Chemical Engineering Journal

www.elsevier.com/locate/cej

Numerical and experimental investigations on liquid mixing in static micromixers

Michael Engler*, Norbert Kockmann, Thomas Kiefer, Peter Woias

Albert-Ludwigs-Universität Freiburg, Georges-Koehler-Allee 102, D-79110 Freiburg, Germany

Received 28 July 2003; accepted 13 October 2003

Abstract

The importance of micromixers for microreaction technology demands some well-founded knowledge on the mixing behaviour of these devices. We show by numerical simulations as well as experimentally that increasing vorticity inside static T-shaped micromixers with rectangular cross-sections occurs even at low Reynolds numbers and that these effects can be used to improve the mixing quality. Hereby we distinguish between three flow regimes. Additionally, we give a new identification number for this kind of problems and we show that this number suits for static T-mixers. This is confirmed by simulations and experimental measurements.

The results will help to understand the mixing process inside microchannels. The overall aim is to develop basic rules for the design and implementation of successful micromixers.

Keywords: T-shaped micromixers; Microreactors; Microreaction technology; CFD-simulation

1. Introduction

Mixers are essential units for reaction technology in common, so for the implementation of microreaction technology, one needs proper micromixers at first. A good and comprehensive overview over mixing in general can, e.g. be found in Harnby et al. [1] or in Bourne [2], the latter mainly concerning mixing with chemical reactions. In recent years, the development of micromixers in MEMS technology has made an enormous progress and the implementation of microprocess units like micromixers and microreactors has come into reach. Several successful implementations of so-called static micromixers have been reported [3,4–6]. These devices operate by splitting the fluid flow into a multitude of fluid segments that mix by diffusion. Some other, so-called active micromixers use external energy applied via mechanical, pneumatic, or ultrasonic forces for the main mixing process [7]. Here, quasi-turbulent effects are induced into the mixers and enhance the mixing quality.

Only a small number of micromixers use convection as the main mixing process. Unfortunately, many of these mixers are still not well understood and a detailed look onto the underlying vortex phenomena is often missing. Especially the examination of the local processes inside of these convective or "vortex" mixers is often not accomplished. This gives the motivation to study these phenomena in more detail.

This paper shows that increasing vorticity can be found in simple T-shaped static micromixers even at low Reynolds numbers of approximately 200 and that these effects can be used to improve the mixing quality. Furthermore, the object of the paper is to describe the fluid flow, the mass transfer, and the mixing in a detailed manner. For this, we have simulated T-mixers with the commercial simulation tool CFD-ACE+ from CFDRC (for more details about this tool, please see http://www.cfdrc.com). We also fabricated a series of micromixers with rectangular cross-sections and have built up a suitable measurement setup to compare the simulation results with the real mixing behaviour. In sum, these first results will be used to model the mixing inside of T-shaped micromixers.

2. Numerical investigations

As mentioned above, we use the commercial numerical tool CFD-ACE+ from CFDRC for simulation of the T-mixers. This tool uses a finite volume method to calculate the flow and the diffusion inside the mixers. The simulations have been performed with approximately

* Corresponding author. Tel.: +49-761-203-7504; fax: +49-761-203-7492.
E-mail address: engler@imtek.de (M. Engler).

1385-8947/$ – see front matter © 2004 Elsevier B.V. All rights reserved.
doi:10.1016/j.cej.2003.10.017

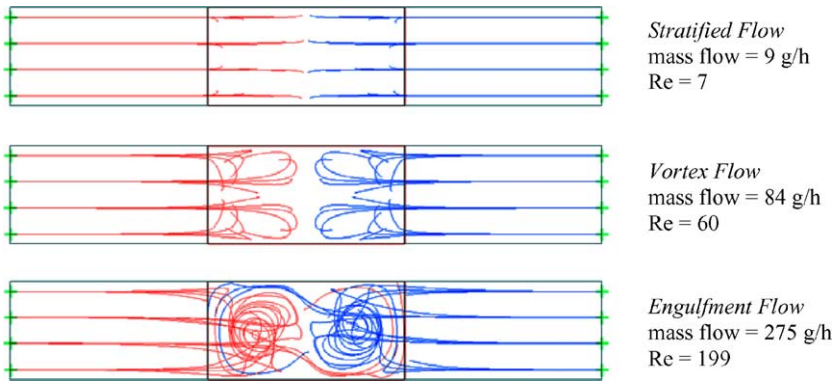

Fig. 1. Streamlines inside a T-mixer (channel widths 300 and 600 μm) at different mass flows. View is into the mixing channel (left and right are the inlet channels).

100,000 elements. As grid elements we used rectangles for the channels and cubes for the mixing chamber where the inlet channels and the outlet channel meet. By using non-linear grids, adjacent grid elements never exceed a volume-to-volume ratio of 1.2 to avoid stability problems and to increase the accuracy of the numerical solution. For the boundary conditions we used a fixed pressure from 2 up to 500 Pa for the inlet channels (symmetrically) and 0 Pa for the outlet channel. The fixed pressure boundary conditions define a fully developed parabolic flow profile at the inlets and the outlet. To achieve realistic simulations, the channels are chosen long enough and hence do not significantly influence the simulation of the fluid behaviour inside the mixer.

2.1. Flow regimes

As already described in [8] there are three different laminar flow regimes which occur inside the mixer. At low flow velocities there is the *stratified flow regime* in which the streamlines are scarcely bent and follow the channel walls, see Fig. 1, top. Inside of this regime mixing is provided by diffusion only. At medium velocities we obtain the second, the *vortex flow regime*. Here, vortices are building up inside the channels. The main mixing principle is still diffusion at the border face of the two fluids. However, the mixing quality is becoming worse due to the higher fluid velocity and therefore shorter residence time for the fluid particles to diffuse. This effect is to some extent compensated by the swirling fluid flow which gives a slightly improved mixing quality by dragging fluid from the middle to the top and bottom side of the mixing channel, see Fig. 1, middle. The flow still shows axial symmetry to the mixing channel. In the third regime, the *engulfment flow regime* at high velocities, this axial symmetry breaks up. The streamlines do no longer meet in the middle of the channels, but intertwine and reach to the opposite side of the wall, see Fig. 1, bottom. This engulfment of the streamlines leads to a very high improvement of the mixing quality.

2.2. Mixing quality

The simulation results allow us to achieve detailed data of the local concentration. These results can be used to calculate an overall mixing quality at a deliberate cross-section of the mixing channel. The mixing quality α is calculated by

$$\alpha = 1 - \sqrt{\frac{\sigma_M^2}{\sigma_{max}^2}}, \tag{1}$$

where σ_{max}^2 is the maximum variance of the mixture (which is 0.5 for symmetrical boundary conditions) and σ_M^2 is defined by

$$\sigma_M^2 = \frac{1}{n}\sum_{i=1}^{n}(c_i - \bar{c}_M)^2, \tag{2}$$

with n being the number of grid points inside the cross-section, c_i the concentration at grid point i and $\bar{c}_M$ being the optimal mixing concentration which is 0.5 for symmetrical boundary conditions. Using Eq. (1), $\alpha = 0\%$ indicates no mixing while $\alpha = 100\%$ indicates perfect mixing. Fig. 2 shows the mixing quality for a 600 × 300 × 300

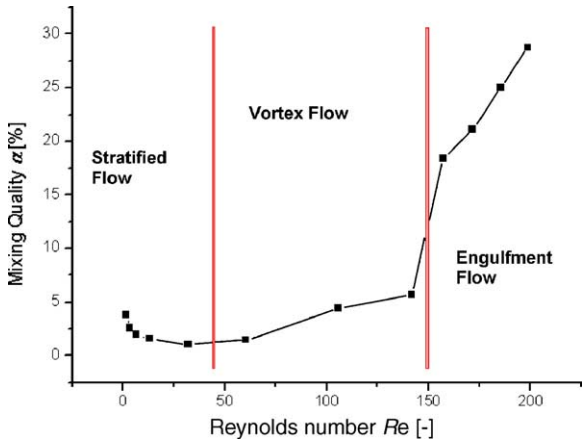

Fig. 2. Mixing quality α over Reynolds number for a 600 × 300 × 300 mixer.

mixer (notation: width of mixing channel in μm × width of inlet channels in μm × depth of all channels in μm) with increasing Reynolds number at a channel position of 1.8 mm downwards the mixing channel. Denoted are the three different flow regimes. The distinction between the stratified and the vortex flow regime is not sharp. To define a suitable limit we have fixed it to the point where the first streamlines are bending for more than 90°. One sees the deterioration of α during stratified flow and the slight improvement in the vortex flow regime. In engulfment flow, a sudden increase of the mixing quality can be observed which origins from the intertwining of the streamlines.

3. Experimental investigations

To support the results acquired from the simulations, first experimental studies were accomplished as well. We have used T-shaped mixers made of silicon which are covered

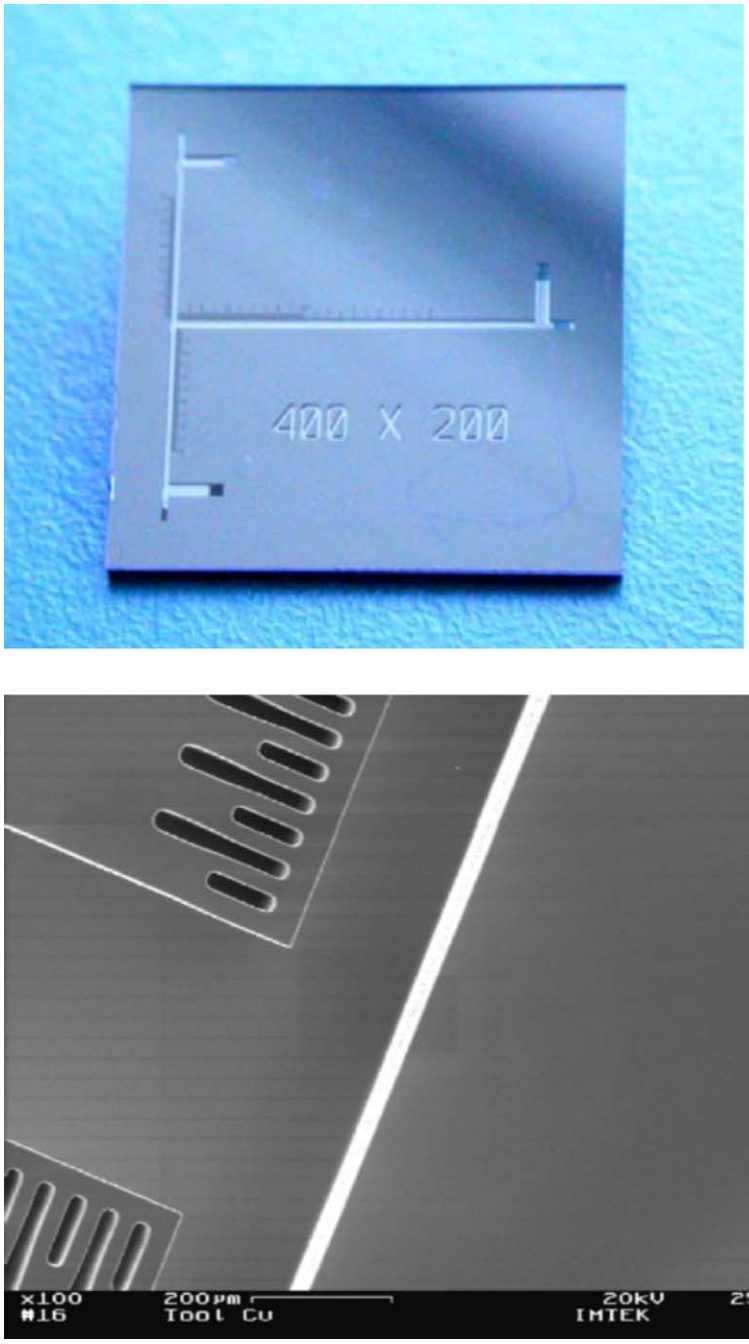

Fig. 3. Photo (top) and SEM picture with 100× magnification (bottom) of a 400 × 200 × 300 T-mixer fabricated by reactive ion etching.

by Pyrex glass. The rectangular channels are fabricated by *reactive ion etching* (RIE). The flow inlets and the outlet are fabricated by anisotropic KOH etching from the chip backside, while the T-channel was made on the front side. The Pyrex glass cover was mounted by anodic bonding to provide a very tight closure. In Fig. 3, a T-mixer chip is shown together with an SEM photo of the mixing chamber. For a better quantification of the results, we have included a length scale along the channels.

3.1. Experimental setup

For the measurements, clear deionised water was used in one and demonised water dyed by Rhodamin B in the other inlet channel. Due to the low concentration of 0.002 mol/l of Rhodamin B in water any influence on the fluid behaviour can be neglected. The mass flow was provided by pressurised vessels and controlled by manually operated valves and a pressure controller. The mean velocities in the inlet channels were measured by inline flow meters. To quantify the pressure, three piezoresistive pressure sensors were used, which measure the pressure directly after the inlets and before the outlet, respectively. For this purpose, additional small channels orthogonal to the inlet channels and the outlet channel were etched into the silicon. These channels have no influence on the fluid behaviour in the mixing zone since they are positioned near the inlets and the outlet, respectively. The mount for the mixer chip and the pressure sensors, see Fig. 4, was fabricated using standard machining. For the sealing, plates made of Perbunan® rubber are used. Together with brackets, which press the mixer onto the Perbunan®, a leak and pressure-tight mounting is provided.

3.2. Measurements

The mixing inside of the micromixers is observed optically with a microscope. At low mass flows, a straight borderline between the two fluids can be found, see Fig. 5, bottom. Looking further along the mixing channel this borderline is broadening up due to diffusion. With increasing mass flow, it can be seen that the borderline is breaking up and that the fluids swap to the other side of the channel. Single filaments of dyed and undyed fluid can be observed, see Fig. 5, bottom. At even higher mass flow, the filaments are disappearing and the colour of the fluid looks very homogenous. Good results are also achieved if the inlet flows are asymmetrical. This shall be subject to further investigations.

For a quantification of the experiments, we measured the pressure with increasing mass flow for different mixers. From that, the beginning of the engulfment flow can easily be derived and compared to the simulations which have been accomplished.

4. Results and discussion

4.1. Identification number

As we have shown in [8], the development of the vortex and the engulfment regime is strongly depending on the geometry. Hence, the Reynolds number is not a good identification number for the distinction of the different regimes, because it only accounts for the ratio between the inertial and the viscous forces and not for the appearance of vortices. Seen from a more abstract point of view, the Reynolds

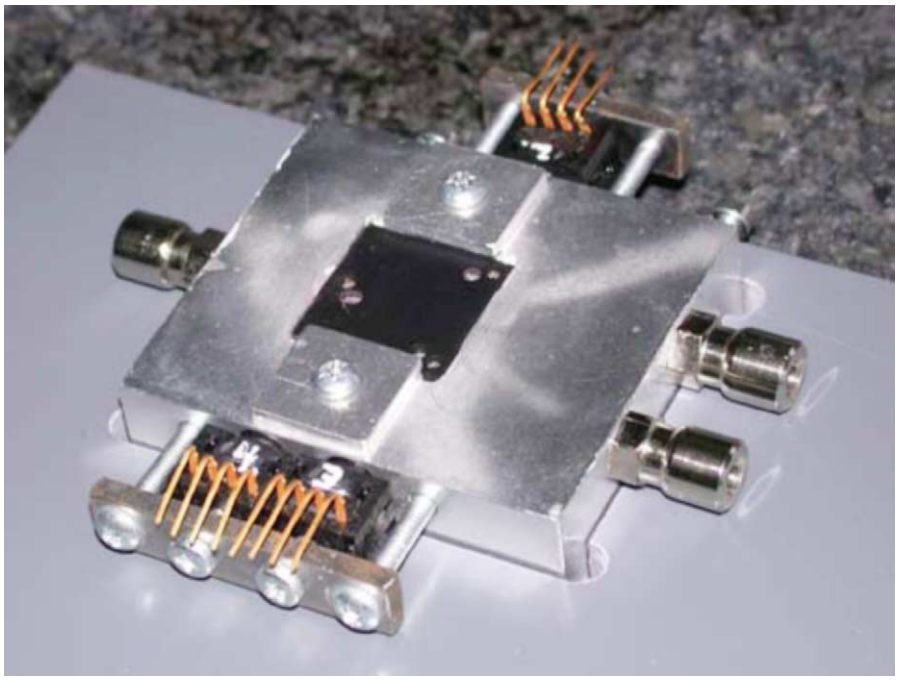

Fig. 4. Photo of the mixer mount.

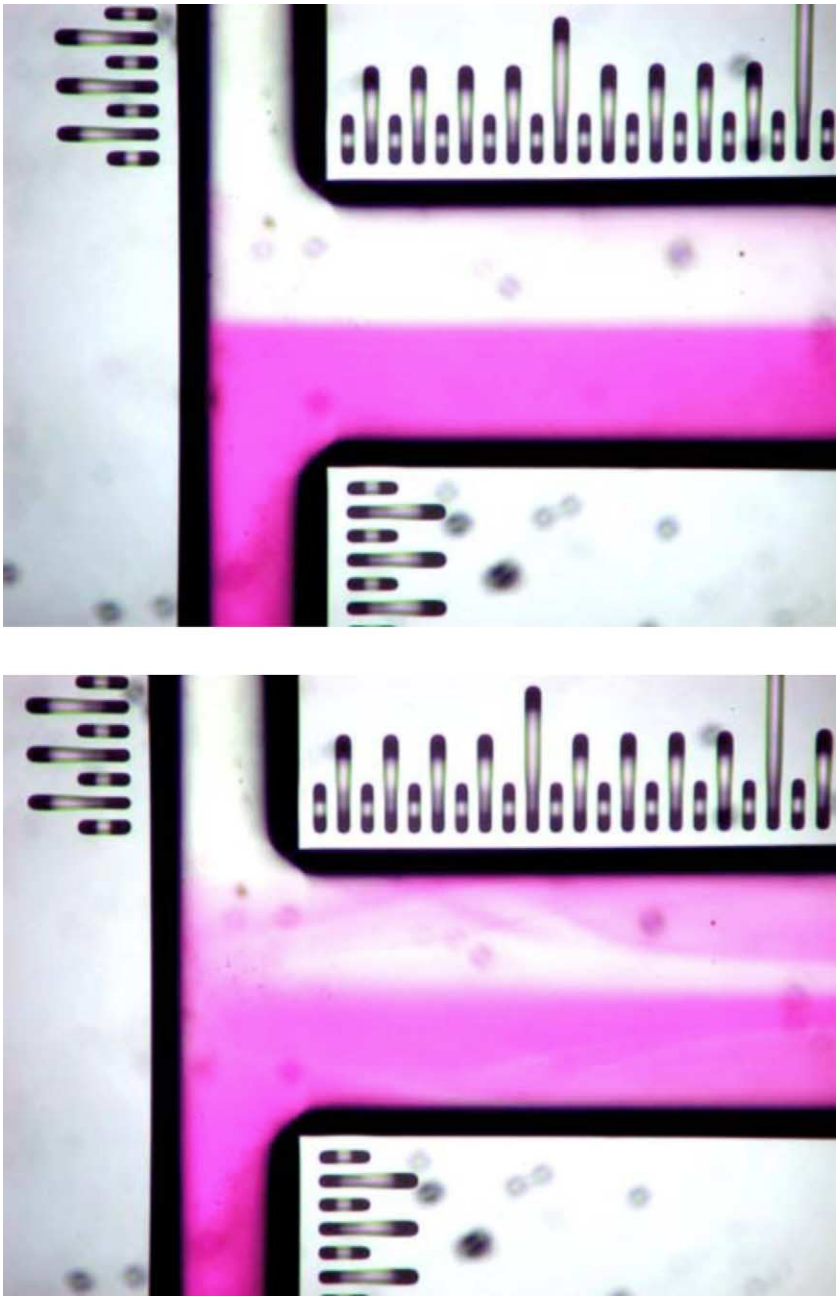

Fig. 5. Measurement of the fluid flow inside a 600 × 300 × 300 mixer at two different mass flows (top: 160 g/h; bottom: 252 g/h) and flow regimes.

number only includes flow, which is the volume flow in fluidics, and disregards effort. We thus need an identification number that also includes the effort, i.e. the energy input, which is corresponding to the pressure loss in fluidics.

To receive a suitable identification number, one can perform a dimensional analysis on the problem. For this, we have chosen the following parameters: the hydraulic diameter d_h, the pressure loss per length $\Delta p/l_V$, mean flow velocity u, the kinematic viscosity ν and the fluid density ρ. Here, l_V is the ratio of the control volume V and the cross-sectional area of the mixing channel A_M. With $Re = d_h u/\nu$ and the Euler number $Eu = \Delta p/\rho u^2$, the dimensional analysis gives the identification number:

$$K = \left(Eu \frac{d_h}{l_V} Re^3 \right)^{1/4}. \quad (3)$$

4.2. Control volume

Special care has to be taken which control volume is chosen for the calculation of K. It should be constrained to a volume where the streamlines are strongly bent. Volumes with laminar readjusted streamlines have to be left out because they do not add to the forming of vortices. As we have seen

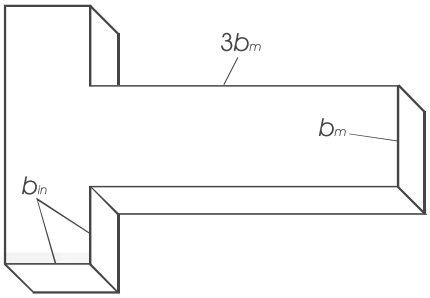

Fig. 6. Control volume for the calculation of K.

from simulations as well as from experiments, the laminar flow in the mixing channel is readjusted after a maximum length of three times the width of the mixing channel. The simulations show that inside the inlet channels the streamlines begin to bend at a distance of about one time the width of the inlet channel before the mixing chamber. From these observations, the control volume shown in Fig. 6 was derived, with b_m denoting the width of the mixing channel and b_{in} denoting the width of the inlet channels.

An interesting correlation concerning K can be observed by the following considerations. For this, we use the ratio of the space available (denoted as the hydraulic diameter of the mixing channel d_h) and the space which is needed for the vortex formation. For the space needed, we have chosen the Kolmogorov length λ_K as a starting point. This parameter origins from turbulence theory and denotes the scale of the smallest eddies in fully developed turbulence which may occur inside a certain fluid volume. It is calculated by

$$\lambda_K = \left(\frac{\nu^3}{\varepsilon}\right)^{1/4}, \tag{4}$$

with ν being the kinematic viscosity of the fluid and ε being the specific energy dissipation inside the fluid. The latter is calculated by

$$\varepsilon = \frac{\Delta p \dot{V}}{m}, \tag{5}$$

where Δp denotes the pressure loss over the control volume V with corresponding mass m and volume flow $\dot{V}$. With this information and with a constant density ρ, d_h/λ_K is calculated by

$$\frac{d_h}{\lambda_K} = \left(\frac{d_h^4\,\Delta p\,\dot{V}}{\nu^3 m}\right)^{1/4} = \left(\frac{d_h^4\,\Delta p\,\rho\dot{m}}{\eta^3 V}\right)^{1/4}, \tag{6}$$

with η being the dynamic viscosity of the fluid. Now, comparing Eq. (6) with Eq. (3) using $\eta = \nu\rho$ and $\dot{m} = \rho A_M u$ yields

$$K = \frac{d_h}{\lambda_K}. \tag{7}$$

Eq. (7) is understandable from a phenomenological point of view. It says that K is the ratio of the hydraulic diameter d_h and a characteristic length denoting the scale of the created vortices inside the channel, here denoted by the Kolmogorov length λ_K. However, this dimensional analysis cannot be finished without further discussion, starting with the critical question whether the combination of parameters from turbulent and non-turbulent regimes is justified. Currently our understanding of K is reasonable as far as the phenomenon itself—vortex formation in a confined geometry—is considered. However, it is clear that more research is needed to evaluate the exact role of λ_K as the situation in a microchannel is different from fully developed turbulence. It has, for example, to be investigated, to which amount the pressure loss inside the control volume contributes to the specific energy dissipation for the vortex formation, as the pressure loss does not only origin from the vortex creation but also from the wall friction of the fluid. Furthermore, the choice of the control volume V has to be examined, as it can heavily influence the value of K. These issues shall be the subject of future research which may lead to the finding of a different length scale for the microchannel situation. We have, nevertheless, carried out a comparison of K with our theoretical and experimental results to get information about the principal feasibility of our approach.

4.3. Measurement results

Using Eq. (6), we are able to calculate d_h/λ_K. The fluid properties ρ and η as well as the geometric parameters d_h and V are known. For d_h and $\dot{m}$, we use the data of the mixing channel and neglect the inlet channels, because they add only little to the control volume. The mass flow can easily be adjusted by the pressure controller, the valves, and the flow meters. The pressure loss is measured by the pressure sensors over the entire mixing chip. So, if we want to receive the pressure loss inside the control volume, we have to subtract the pressure loss which origins from the channels. This is necessary because the inlet channels and the outlet channel are so long that measurements over the whole chip would highly influence the results. According to [9], the pressure loss inside a straight channel i with constant cross-section is calculated by

$$\Delta p_i = \frac{\zeta_i l_i \eta \dot{m}_i}{2 d_{h,i}^2 \rho A_i}, \tag{8}$$

with l_i denoting the length of the channel i, $d_{h,i}$ its hydraulic diameter, A_i the area of its cross-section, $\dot{m}_i$ the mass flow through the channel and ζ_i a correction factor for the geometry of the cross-section. The latter can be calculated for a rectangular channel to

$$\zeta_i = \sum_{k,l=1;\,\mathrm{odd}}^{\infty} \frac{\beta_i^2 + 2\beta_i + 1}{k^2 l^2 (k^2 + \beta_i^2 l^2)}, \tag{9}$$

where β_i is the ratio between the two sides of the cross-section of the channel i. This equation is received from solving the Navier–Stokes equations for a straight

Table 1
d_h/λ_K, mass flow and pressure loss inside the control volume at the beginning of engulfment for different mixer geometries

Mixer chip	*Re*	d_h/λ_K at beginning of engulfment	Mass flow $\dot{m}$ (g/h)	Δp (Pa)
1600 × 400 × 300	87	46	257.5	191
1000 × 500 × 300	235	42	448.7	465
1000 × 500 × 200	271	47	489.5	1505
600 × 300 × 300	147	34	198.5	277
400 × 200 × 200	75	45	69.2	3475
200 × 100 × 100	135	46	64.3	762

rectangular channel with stationary laminar flow. With $p_{in,1}$ and $p_{in,2}$ as the measured pressures at the inlets and p_{out} as the measured pressure at the outlet, Δp is then calculated to

$$\Delta p = \tfrac{1}{2}(p_{in,1} - \Delta p_1) + (p_{in,2} - \Delta p_2) - (p_{out} + \Delta p_3), \tag{10}$$

with *i* denoting the three channels (two inlets and one outlet).

We have carried out measurements for six different mixers. Here we have measured the beginning of the engulfment because this can be distinguished from vortex flow in a proper manner. From these results we have calculated the identification number d_h/λ_K for each mixer as shown in Table 1.

We can see that the Reynolds number is not a good identification number for this problem, because it varies widely. However, we see a rather constant value of d_h/λ_K of around 40 for the transition from vortex (symmetric) to engulfment (asymmetric) flow. These results seem to confirm the assumption that we have found an identification number which predicts the vortex creation inside microchannels with at least some accuracy and which is independent from geometry. Keeping in mind the complicated calculation of this number and all other critical issues discussed before it is surprising that the experimental results fit in such a good manner. However, more work has to be done to justify the exact composition of *K*.

4.4. Numerical results and comparison with measurements

We have also analysed the data of the simulations of a 600 × 300 × 300 mixer and compared it with the measurements of the same geometry. Some results are listed up in Table 2.

A comparison of the simulation results (first engulfment) with the measurement results of the 600 × 300 × 300 mixer shows a very good agreement. In both measurement and simulation, d_h/λ_K is nearly at the same value and, additionally, the mass flow $\dot{m}$ and the pressure loss Δp match very well with a deviation of only 10%. This agreement is a very good result as it helps to confirm the correctness of the measurements and simulations. Of course it has to be approved by more simulations for different geometries and by further measurements. This will be subject to future investigations.

Table 2
d_h/λ_K, mass flow and pressure loss inside the control volume with increasing Reynolds number for the 600 × 300 × 300 mixer

Flow regime	*Re*	d_h/λ_K	Mass flow $\dot{m}$ (g/h)	Δp (Pa)
Laminar	6.6	6.2	9.1	6.1
Laminar	32	13.8	44.3	30.9
Vortex	60	19.4	83.5	64.3
Vortex	142	32.3	196.3	212.0
Engulfment (first)	157	34.5	217.6	247.3
Engulfment	199	40.3	275.3	364.8

5. Conclusion and outlook

Our investigations on static T-shaped micromixers have given some results for the understanding of the underlying processes inside of these mixers. The three different flow regimes, stratified laminar flow, vortex flow and engulfment flow, which we have already simulated in earlier work, have been confirmed by experimental investigations. Especially the appearance of the engulfment flow has been demonstrated in a very good manner. We have further shown that the identification number d_h/λ_K is suitable—at least on a phenomenological basis—to describe this kind of problem. In our micromixers engulfment flow will typically happen when d_h/λ_K achieves values above 40. We have also found a very good agreement between simulation and experiment which confirms the correctness of the results.

Future investigations will contain simulations of different geometries. Further measurements of the mixers will also be made. The composition of *K* is still an open question which has to be discussed in the future. This altogether will help to approve these first experiments and simulations and to strengthen the results we have given in this paper. Asymmetrical boundary conditions are also worth to be examined as they seem to improve the mixing quality better than symmetrical boundary conditions. The final aim is to develop basic rules for the design and implementation of a successful micromixer.

Acknowledgements

We gratefully acknowledge the DFG “Deutsche Forschungsgemeinschaft” for their financial support in the priority program SPP 1141 *Mischung*.

References

[1] N. Harnby, M.F. Edwards, A.W. Nienow, Mixing in Process Industries, Butterworths/Heinemann, Oxford, 1992.
[2] J.R. Bourne, Mixing and the selectivity of chemical reactions, Organic Process Research & Development 2003, vol. 7, ACS Publications, pp. 471–508.
[3] W. Ehrfeld, V. Hessel, H. Löwe, Microreactors—New Technology for Modern Chemistry, Wiley/VCH, Weinheim, 2000.

[4] V. Hessel, H. Löwe, Mikroverfahrenstechnik: Komponenten—Anlagen-konzeption—Anwenderakzeptanz—Teil 1, Chemie Ingenieur Technik 74 (2002) 17–30.
[5] V. Hessel, H. Löwe, Mikroverfahrenstechnik: Komponenten—Anlagen-konzeption—Anwenderakzeptanz—Teil 2, Chemie Ingenieur Technik 74 (2002) 185–207.
[6] V. Hessel, H. Löwe, Mikroverfahrenstechnik: Komponenten—Anlagen-konzeption—Anwenderakzeptanz—Teil 3, Chemie Ingenieur Technik 74 (2002) 381–400.
[7] P. Woias, K. Hauser, E. Yacoub-George, An active silicon micromixer for μTAS applications, in: Proceedings of the μTAS'00 Workshop, Kluwer Academic Publishers, Dordrecht, 2000, pp. 277–282.
[8] N. Kockmann, M. Engler, C. Föll, P. Woias, Liquid mixing in static micromixers with various cross sections, in: Proceedings of the First International Conference on Micro Minichannels, ASME, Rochester, NY, 2003.
[9] M. Gad-el-Hak (Ed.), The MEMS Handbook, CRC Press, Boca Raton, 2001 (Chapter 6).